CRYSTAL GROWTH & DESIGN

Article

pubs.acs.org/crystal

Bond Formation upon Water Removal in an Unusual "Pseudo"-Topotactic Reaction Investigated by Single-Crystal Structure and in Situ Synchrotron X-ray Powder Diffraction Analysis

Joanna Dopta,[†] Anna-Lena Hansen,[†] Nicole Pienack,[†] Lisa K. Mahnke,[†] Helge Reinsch,[†] Martin Etter,[‡] Christian Näther,[†] and Wolfgang Bensch*,[†]

[†]Institute for Inorganic Chemistry, Christian-Albrechts-University of Kiel, Max-Eyth-Str. 2, 24118 Kiel, Germany

[‡]Deutsches Elektronen-Synchrotron, Notkestr. 85, D-22607 Hamburg, Germany

Supporting Information

ABSTRACT: The new compound $[Cu(cyclam)(H_2O)]\{[Cu(cyclam)]_2[HTiNb_9O_{28}]\}\cdot 26H_2O$ (**1**) (cyclam = 1,4,8,11-tetraazacyclotetradecane) was obtained under solvothermal conditions. Its crystal structure contains a monotitano-nonaniobate anion in which one position is equally occupied by Nb(V) and Ti(IV). The anions are expanded by $[Cu(cyclam)]^{2+}$ cations via Nb−O−Cu bridges generating $\{[Cu(cyclam)]_2[HTiNb_9O_{28}]\}^{2-}$ cluster units, which are arranged into layers. Between these layers there are additionally isolated $[Cu(cyclam)(H_2O)_2]^{2+}$ cations as well as hydrate water molecules. Storage of **1** at room temperature leads to loss of ∼13 water molecules, and a new crystalline phase (**2**) crystallizes that, with heating, transforms into the anhydrate. The reversibility of this reaction was investigated by thermogravimetry and X-ray powder diffraction (XRPD). Temperature-dependent in situ synchrotron XRPD investigations prove an abrupt phase transition, in which especially the *a* axis is dramatically shortened and the $\{[Cu(cyclam)]_2[HTiNb_9O_{28}]^{2-}\}$ cluster is rearranged. Single-crystal X-ray diffraction of **2** reveals that, despite the unusual large shrinking of the unit cell volume, the domains formed by water removal exhibit some preferred orientation close to that expected for a topotactic reaction, which allowed the performance of a structure analysis. In the structure of **2**, the two water molecules of the isolated $[Cu(cyclam)(H_2O)_2]^{2+}$ cation in **1** are replaced by two terminal cluster O atoms, leading to the formation of chains via Nb−O−Cu bonds, and this phase transition is accompanied by an ordering of one of the two cyclam ligands.

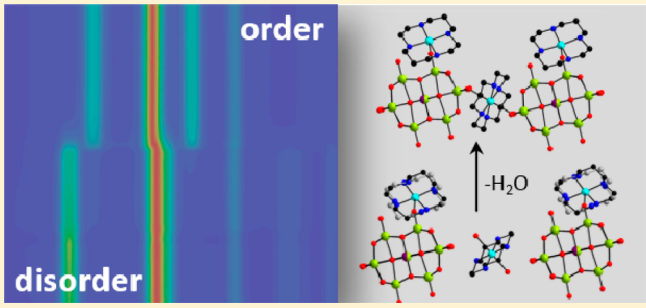

INTRODUCTION

Solid compounds containing crystal water molecules are potentially precursors or educts for the preparation of new, water-deficient crystalline phases by, for example, directed thermal decomposition reactions. A very prominent example is $CuSO_4\cdot 5H_2O$, which can be thermally dehydrated in three distinct steps including formation of the crystalline intermediates $CuSO_4\cdot 3H_2O$, $CuSO_4\cdot H_2O$, and $CuSO_4$.[1−3] Another example is $CaSO_4\cdot 2H_2O$, which can be thermally dehydrated to the semihydrate and finally to anhydrite.[4−6] In this context, it is noted that there are an increasing number of reports that deal with reversible solvent removal.[7−11]

In most cases the intermediates obtained by water removal from especially more complex hydrated structures were normally not structurally characterized, because only polycrystalline powders are obtained. Because the composition changes during dehydration such reactions do not proceed via a second-order single crystal to single crystal phase transition, for which a crystallographically group−subgroup relation is required. Usually they are of first order and proceed via nucleation and growth of a new crystalline phase, leading to the formation of domains, without changing the crystal morphology. In most cases there is no structural relationship between the hydrate and the intermediate phase, and therefore, the domains show a random orientation, and the diffraction pattern corresponds to that of a powder. However, in very few cases there is a strong relationship between the structures of the reactant and the product, and in this case the domains formed in a reaction exhibit a strong preferred orientation simulating the diffraction pattern of a single crystal. The presence of such a reaction, called topotactic, can only be proven by single-crystal X-ray diffraction, and in ideal cases differences between the diffraction pattern of the pristine and the product phase are only detected in the mosaic spread.[12−15] For such reactions the question arises what will happen if larger structural changes occur for which the orientation of the domains are far from perfect and if structural information can be retrieved in such cases. In the course of our ongoing

Received: June 7, 2019
Revised: July 25, 2019
Published: August 26, 2019

DOI: 10.1021/acs.cgd.9b00727
Cryst. Growth Des. XXXX, XXX, XXX−XXX

investigations on the synthesis and properties of new polyoxometalates we found such an example.

Polyoxometalates (POMs; M = V, Nb, Ta, Mo, and W) are an important class of compounds that is characterized by a large variety of high-nuclearity cluster anions exhibiting different chemical compositions, properties, shapes, sizes, and topologies.[16−30] In most cases POMs contain an appreciable amount of water, which in several cases is emitted already at room temperature. Focusing on polyoxoniobates (PONb), examples include $K_{12}[Ti_2O_2][SiNb_{12}O_{40}]\cdot 16H_2O$,[31] $Na_{14}[H_2Si_4Nb_{16}O_{56}]\cdot 45.5H_2O$,[31] $Li_7K[Nb_6O_{19}]\cdot 15H_2O$,[32] $Li_{13}K[SiNb_{12}(OH)_2O_{38}]\cdot 17H_2O$,[32] $(TMA)_9[V_3Nb_{12}O_{42}]\cdot 18H_2O$ (TMA = tetramethylammonium),[33] $Na_7[HNb_6O_{19}]\cdot 15H_2O$,[34] $[Cu(en)_2(H_2O)_2]_5K_{10}[K(GeOH)_2Ge_2Nb_{16}H_3O_{54}]_2\cdot 38H_2O$ (en = ethylenediamine),[35] $[Cu(en)_2]_3\{[Cu(en)_2][H_6SiNb_{18}O_{54}]\}\cdot 22H_2O$,[36] $(TMA)_5[H_2TeNb_5O_{19}]\cdot 20H_2O$,[37] $(TMA)_5[H_3Nb_6O_{19}]\cdot 20H_2O$,[38] $H_4Na_6K_{22}Cs_4[H_4Nb_{52}O_{150}]\cdot 63H_2O$,[39] $Na_{12}[Pt(Nb_6O_{19})_2]\cdot 52H_2O$.[40] We note that this list of compounds is not complete, and we are also aware that PONb compounds with a lower number of crystal water molecules were also reported. In most cases the thermal stability and water removal of the samples was investigated with thermoanalytical methods, but no further efforts were undertaken to characterize partially or fully dehydrated decomposition products in more detail. In some reports the authors mentioned that the samples tend to lose water already at room temperature when removed from the mother liquor like, for example, $[N(CH_3)_4]_4[Na_2Nb_{10}O_{28}]\cdot 8H_2O\cdot 1/2CH_3OH$,[41] $[N(CH_3)_4]_6[Nb_{10}O_{28}]\cdot 6H_2O$[41] or $Na_8[Nb_8Ti_2O_{28}]\cdot 34H_2O$,[42] but even here no further investigations were performed. This means that the synthetic potential of hydrated PONbs as starting materials for the generation of new, water-deficient compounds was not explored until now.

In this context we reported on the reversible dehydration and rehydration of $\{[Cu(cyclam)(H_2O)]_2[Cu(cyclam)]_2[Nb_{10}O_{28}]\}_n\cdot 9nH_2O$ (cyclam = 1,4,8,11-tetraazacyclotetradecane), which is accompanied by a significant change of the crystal structure,[43] but the pristine material could be recrystallized upon water uptake. In further investigations we synthesized a novel compound with the composition $[Cu(cyclam)(H_2O)]_2\{[Cu(cyclam)]_2[HTiNb_9O_{28}]\}\cdot 24H_2O$ (**1**), which was obtained by solvothermal reaction. After the crystals were removed from the mother liquor, cocrystallized H_2O molecules are partially emitted, leading to formation of a new compound with composition $\{[Cu(cyclam)]_3[HTiNb_9O_{28}]\}_n\cdot \approx 13H_2O$ (**2**) as intermediate that does not transform back into **1** in a humid atmosphere. This reaction was studied using different methods, including temperature-dependent in situ synchrotron radiation-based X-ray powder diffraction (XRPD) and single-crystal X-ray diffraction to gain detailed information on the structural changes that are accompanied by this reaction.

■ EXPERIMENTAL SECTION

General. All chemicals except $K_7HNb_6O_{19}\cdot 13H_2O$ were purchased and used without further purification: 1,4,8,11-tetraazacyclotetradecane (98+%, Alfa Aesar), $Cu(NO_3)_2\cdot 3H_2O$ (>99%, Merck), $Ti(O^iPr)_4$ (>98%, Merck). $K_7HNb_6O_{19}\cdot 13H_2O$ was synthesized by a literature method.[44] All reactions were performed under hydrothermal conditions in DURAN glass tubes with an inner volume of 11 mL at T = 130 °C for 3 h under stirring. After the reaction products were cooled in an ice bath, the reaction mixtures were filtered off, the mother liquors were transferred into straight glass tubes, and the solvent was left to evaporate at room temperature. The resulting products were washed with very small amounts of demineralized water and stored in air. Larger crystals are relatively stable over a longer period of time, while smaller and/or ground crystallites immediately lose crystal water molecules leading to an opaque solid.

Synthesis. $K_7HNb_6O_{19}\cdot 13H_2O$ (0.2 mmol), 0.4 mmol of $Cu(NO_3)_2\cdot 3H_2O$, and 0.4 mmol of 1,4,8,11-tetraazacyclotetradecane (cyclam) were placed in a DURAN glass tube, and after addition of 3 mL of H_2O and 0.034 mmol of $Ti(O^iPr)_4$, the pH value was adjusted with 0.2 mL of 1 M KOH to ∼11. After slow evaporation of the solvent, violet block-shaped crystals were obtained and were washed with minute amounts of distilled water. Yield: 137.0 mg (46% based on Nb).

Single-Crystal Structure Analysis. Single-crystal X-ray intensity data were collected with an STOE Imaging Plate Diffraction System (IPDS-1) with Mo Kα radiation (λ = 0.710 73 Å) at 170 K. A numerical absorption correction was performed. The crystal structures were solved with SHELXS-97[45] and refined against F^2 using SHELXL-2014.[46] All non-H atoms except some of the disordered water O atoms of lower occupancy were refined anisotropically. The C−H and N−H H atoms were positioned with idealized geometry and refined isotropically with $U_{iso}(H) = 1.2\ U_{eq}(C)$ using a riding model. The O−H H atoms were not located but considered in the calculation of the molecular formula and the molecular weight. One cyclam ligand in compound **1** was disordered in two orientations and was refined with restraints using a split model. The water O atoms are also disordered, and some positions were not fully occupied. For compound **2** internal R-value as well as all other reliability factors including the residual electron density are high, because the intensities could not be integrated with high accuracy. Selected crystal data and details of the structure refinement are listed in Table 1.

CCDC-1919265 (**1**) and CCDC-1919264 (**2**) contain the supplementary crystallographic data, which can be obtained free of charge via www.ccdc.cam.ac.uk/data_request/cif.

Table 1. Selected Crystal Data and Details of the Structure Refinement for 1 and after Storing This Crystal for 3 d at Room Temperature

compound	**1**	**2**
formula	$C_{30}H_{125}Cu_3N_{12}Nb_9O_{54}Ti$	$C_{30}H_{125}Cu_3N_{12}Nb_9O_{41}Ti$
molecular weight/g mol^{-1}	2593.12	2361.94
crystal system	monoclinic	monoclinic
space group	$P2_1/c$	$P2_1/c$
a/Å	16.7690(4)	14.5725(10)
b/Å	17.5766(3)	17.6063(7)
c/Å	15.6167(4)	15.1513(10)
a/deg	90	90
β/deg	113.746(2)	108.702(5)
γ/deg	90	90
V/Å^3	4213.21(17)	3682.1(4)
T/K	170(2)	200(2)
Z	2	2
D_{calc}/g cm^{-3}	2.044	2.130
μ/mm^{-1}	2.107	2.387
θ_{max}/deg	26.005	26.005
measured refl	38 866	27 325
unique refl	8257	7164
refl $F_0 > 4\sigma(F_0)$	7303	5598
parameter	639	448
R_{int}	0.0270	0.1553
R_1 [$F_0 > 4\sigma F_0$)]	0.0370	0.1069
wR_2 [all data]	0.1100	0.2954
GOF	1.054	1.082
$\Delta\rho_{max/min}$/e Å^{-3}	1.019/−0.644	3.686/−1.350

DOI: 10.1021/acs.cgd.9b00727
Cryst. Growth Des. XXXX, XXX, XXX−XXX

In-House X-ray Powder Diffraction. Laboratory X-ray powder patterns were recorded with Cu Kα1 radiation (λ = 1.5406 Å) in transmission geometry on an STOE Stadi-P powder diffractometer with a Ge monochromator and a Mythen 1K detector.

Synchrotron X-ray Diffraction. Synchrotron XRPD was performed at the PETRA III, P02.1 beamline (DESY, Hamburg), between room temperature and 65 °C using a nitrogen gas blower and 60 keV radiation (λ = 0.20717 Å). To determine the detector characteristics, the sample-to-detector distance (SDD), LaB_6 was used as calibration standard. For XRPD, the SDD was 1012.18 mm. The samples were measured in Kapton capillaries. To obtain the water-rich compound, the solid sample of the water-poor material was suspended in water, and the suspension was transferred via syringe into the capillaries. The integration of the scattering data was performed using Fit2D.[47] Desy data helper and Multi power X-ray diffraction data tool for data integration and plotting were applied.

Spectroscopic Investigations. A Bruker Alpha-P ATR IR spectrometer was used to record mid-infrared (MIR) spectra in a range of 400−4000 cm^{-1}. UV−Vis diffuse reflectance spectra were collected on a UV−vis−NIR (NIR = near-infrared) two-channel spectrometer Cary 5 from Carian Techtron Pty using $BaSO_4$ as reference. The IR spectrum and the band assignment are displayed in the Supporting Information.

Elemental Analysis. CHN analyses were done with an EURO EA elemental analyzer (EURO VEKTOR).

Thermal Analysis. Thermogravimetric data were recorded on a Netzsch STA 4096 CD in air with a heating rate of 4 °C/min.

■ RESULTS AND DISCUSSION

Synthetic Aspects. Because alkaline pH values are required for the synthesis of PONbs, one strategy to obtain new compounds with transition-metal (TM) complexes is to prevent the formation of hydroxides by in situ complex formation applying amine molecules.[48] $[Co(en)]^{2+}$ and $[Cr(en)]^{2+}$ cations were the first complexes that were used as counterions in PONbs.[49] In the meantime, a relatively large number of PONbs containing Cu^{2+}-centered complexes were reported, which may be due to the high stability constants of Cu^{2+} amine complexes and the Jahn−Teller distortion of Cu^{II}, which results in flexible coordination geometries.[50]

The title compound was obtained at 130 °C after a reaction time of 3 h. The slurry was stirred during the reaction, and the product crystallized as a violet microcrystalline powder and could be recovered by filtration immediately after solvothermal treatment. Single crystals were grown either by keeping the filtrate at room temperature for several days, allowing the solvent to evaporate slowly, or by heating the mixture of the starting materials hydrothermally without stirring.

Crystal Structure of 1. $[Cu(cyclam)(H_2O)_2]\{[Cu(cyclam)]_2[HTiNb_9O_{28}]\}\cdot 24H_2O$ (**1**) crystallizes in the monoclinic space group $P2_1/c$ with two formula units in the unit cell (Table 1). All atoms, except Cu2, are located on general positions. The structure consists of the monotitanononaniobate $[HTiNb_9O_{28}]^{6-}$ anion and two crystallographically independent $[Cu(cyclam)(H_2O)_2]^{2+}$ (x = 0,1) cations (Figure 1).

The anion is composed of 10 Ti/NbO_6 octahedra sharing common edges, with the central positions occupied with 50% Nb^V and Ti^{IV}. Bond valence sum (BVS) calculations reveal oxidations states of +5 for Nb and +4 for Ti and indicate that the cluster is monoprotonated; a BVS analysis provides an average value of 1.6 for the terminal O atoms (Table S1), and therefore it is highly likely that the proton is spread over these atoms, which is not unusual in polyoxometalate chemistry.

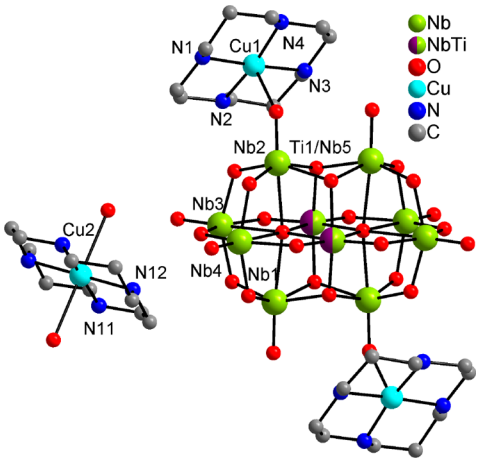

Figure 1. View of the structural units in **1**. The disorder of the cyclam molecule is not displayed, H atoms are omitted, and only selected atoms are labeled.

The geometric parameters, Ti/Nb−O bonds, and O−Ti/Nb−O angles are in the range reported in literature (Table S2).[41,51−53] The $[HTiNb_9O_{28}]^{6-}$ anion is decorated by two symmetry-equivalent $[Cu(cyclam)]^{2+}$ complexes via Nb−O−Cu bridges (Cu1−O5: 2.342(3) Å), thus forming $\{[Cu(cyclam)]_2[HTiNb_9O_{28}]^{2-}\}$ cluster anions. The $Cu1N_4O$ square pyramid is slightly distorted as evidenced by the angles around the Cu^{2+} cation (Table S3). The corresponding cyclam molecule is disordered and was refined using a split model. The second crystallographically independent Cu^{2+} cation is in a distorted octahedral coordination of the four N atoms of the cyclam ligand and two H_2O molecules (Table S3). The $\{[Cu(cyclam)]_2[HTiNb_9O_{28}]\}$ clusters are arranged in layers parallel to the b/c-plane, which are separated by crystal water molecules and $[Cu(cyclam)(H_2O)_2]^{2+}$ cations (Figure 2).

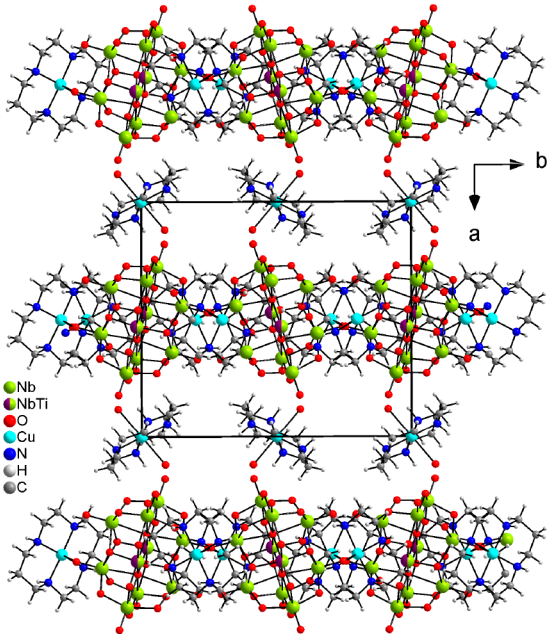

Figure 2. Crystal structure of **1** with view along the c-axis. The disorder of the cyclam ligand and the O atoms of H_2O molecules are not shown.

DOI: 10.1021/acs.cgd.9b00727
Cryst. Growth Des. XXXX, XXX, XXX−XXX

Within the layers, each $\{HTiNb_9O_{28}\}$ cluster is surrounded by four Cu^{2+} cations in a square-planar manner (Figure 3) with the nearest possible distance being too long for bonding interactions (Cu1−O9: 3.70 Å). A more detailed structure description with additional drawings is provided in the Supporting Information and Figures S1−S4.

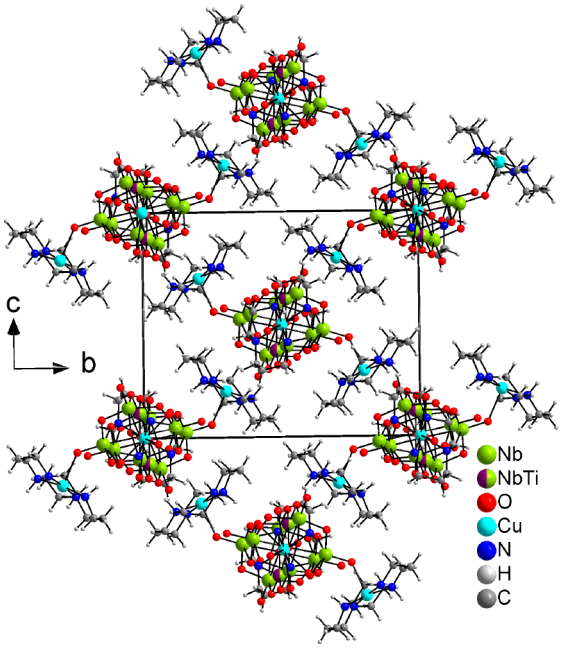

Figure 3. View of the crystal structure of **1** along the crystallographic *a*-axis. The disorder of the cyclam ligand and the water molecules are omitted.

Investigations on the Stability and Water Removal of 1. To investigate the stability of **1** a sample of this compound was placed on a balance leading immediately to a continuous decrease of the sample mass. Therefore, pure samples of **1** can only be obtained if the samples are immersed in a tiny amount of water as shown by XRPD (Figure S5). If the residue obtained after storing compound **1** at ambient conditions is investigated by XRPD, obviously significant changes took place, indicative from the formation of a new crystalline phase (**2**) (Figure S6), also confirmed by time-dependent in-house XRPD measurements (Figure 4).

If **2** residue is stored in a humid atmosphere no transformation into **1** is observed, indicating that this process is not reversible under these conditions (Figure S7). However, compound **2** can be transformed back into **1** by submersing the sample in a water-filled glass tube overnight, protecting the sample by adhesive tape and immediately measured or by suspending the compound in a small amount of water and transferring it into Kapton capillaries. Note that only minute amounts of water were used, because the compound is soluble in water. Both approaches yielded samples showing XRPD patterns similar to that calculated from single-crystal data for **1** (Figure 4 and Figure S7).

Thermogravimetric (TG) measurements of the new phase **2** to 975 °C show three reasonable resolved mass loss steps of ∼10.2, 23.0, and 2% (Figure S8). From the derivative thermogravimetry (DTG) curve it is indicated that the first reaction consists of several steps that cannot be successfully resolved. The mass loss in the first step corresponds to that calculated for the endothermic removal of ∼13 water molecules ($\Delta m_{calc}(-13\ H_2O) = 9.9\%$). Therefore, compound **2** should represent a trideca hydrate, which is in reasonable agreement with the results of an elemental analyses (calcd: C 15.3, H 4.2, N 7.1; found: C 15.0, H 4.0, N 7.0%).

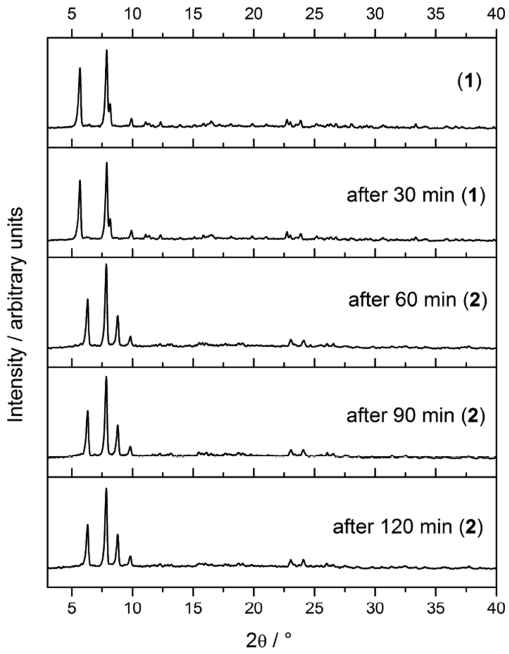

Figure 4. Time-dependent XRPD patterns of **1**.

To investigate the anhydrate formed by the water removal a second TG run was performed and stopped at ∼150 °C, where all the water is removed. XRPD investigations reveal that the powder pattern is completely different from those of **1** and **2**, indicating enormous structural changes (Figure S9). However, stirring the anhydrate in H_2O results in formation of **1**; that is, this structural change is reversible (Figure S10).

In Situ Temperature-Resolved Synchrotron XRPD Investigations. To investigate the transition of **1** into **2** in more detail, experiments using in situ temperature-dependent X-ray diffraction were performed. Therefore, a sample of **1** immersed in tiny amounts of water (see Experimental Section for details) were heated to 40 °C, and the temperature was increased in steps of 2 °C (Figure 5). The XRPD patterns collected at room temperature and at 40 °C prove the presence of compound **1**. Up to ∼50 °C the reflections do not exhibit significant shifts, but the 100 reflection shows an intensity fading. Between 52 and 54 °C reflections of **1** disappear, and new reflections occur. Further heating of the sample to 60 °C induces no further changes of the XRPD pattern. The abrupt change of the powder patterns during the transformation of **1** into **2** is surprising, because as mentioned above such transitions usually proceed via nucleation and growth of a new phase for which some nucleation energy is needed, and because each nuclei has its own predetermined transition temperature, usually both phases coexist over a larger temperature range.

After it was heated to 65 °C, the sample was cooled to room temperature leading to no changes in the XRPD pattern, which indicates that this reaction is irreversible (Figure S11).

However, the changes of the lattice parameters XRPD patterns were evaluated by Pawley refinements (Figure 6). When heated to 44 °C, especially the *b*- and *c*-axes as well as

DOI: 10.1021/acs.cgd.9b00727
Cryst. Growth Des. XXXX, XXX, XXX−XXX

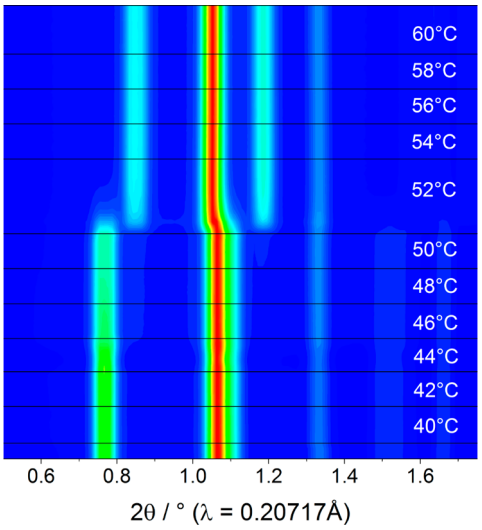

Figure 5. Evolution of the reflection intensities with increasing temperature recorded on a sample of compound **1** suspended in water when heated from 40 to 60 °C. Note that the pattern at T = 52 °C was measured for a longer time.

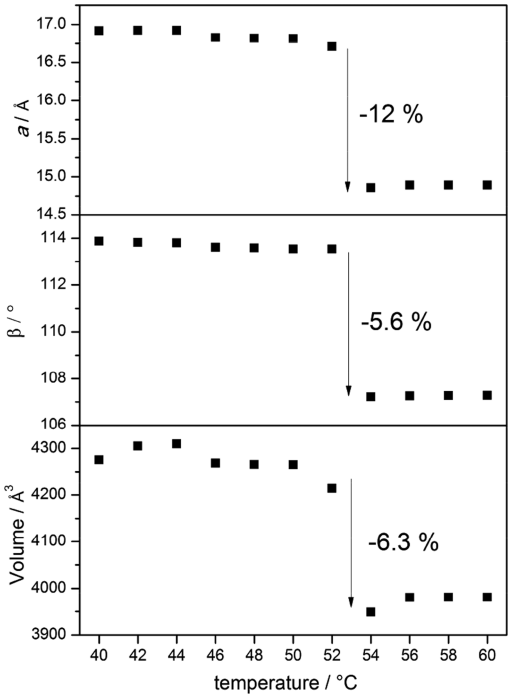

Figure 6. Changes of the a-axis, the angle β, and the unit cell volume as a function of temperature for **1**. Given is the change (in %). For the other parameters see Figure S12.

the unit cell volume slightly increase because of thermal expansion (Figure 6 and Figure S12). At ∼46 °C there is a small anomaly, which can be seen especially in the changes of the c-axis and which is accompanied by a very small decrease of the unit cell volume. It is difficult to decide whether these changes are within the experimental error or if a further transition is involved. At ∼51 °C the structure changes abruptly, obviously because of the water removal leading to discontinuous change of the unit cell volume typical for a first-order phase transition. During this reaction especially the a-axis and the angle β decreases dramatically, whereas the lengths of the b-axis increases (Figure 6).

X-ray Single-Crystal Investigations. The in situ XRPD investigations reveal that the water removal leads to a dramatic change of the unit cell parameters, which indicates enormous structural changes during the phase transition. Therefore, one would assume that there is no strong relationship between the crystal structures of **1** and **2**, which means that this reaction should not be topotactic. However, a closer look reveals that especially the interlayer distance decreases as indicated by the abrupt shortening of the a-axis and that the cations within these layers are rearranged, which can be seen by the change of the angle β. Therefore, the overall structural changes might be much smaller than expected, which means that both structures might be related and that also no change of the space group might be required. To investigate this question in more detail, data collection of a crystal of **1** was performed, and after this crystal was stored at room temperature for 3 d, the measurement was repeated again. Surprisingly, this crystal still diffracted, but the overall crystallinity was very poor, and all reflections were extremely broadened. This is especially obvious by comparison of reciprocal space plots before and after storage, but it is indicated that after water removal some order is still present (Figure 7 and Figures S13−S15).

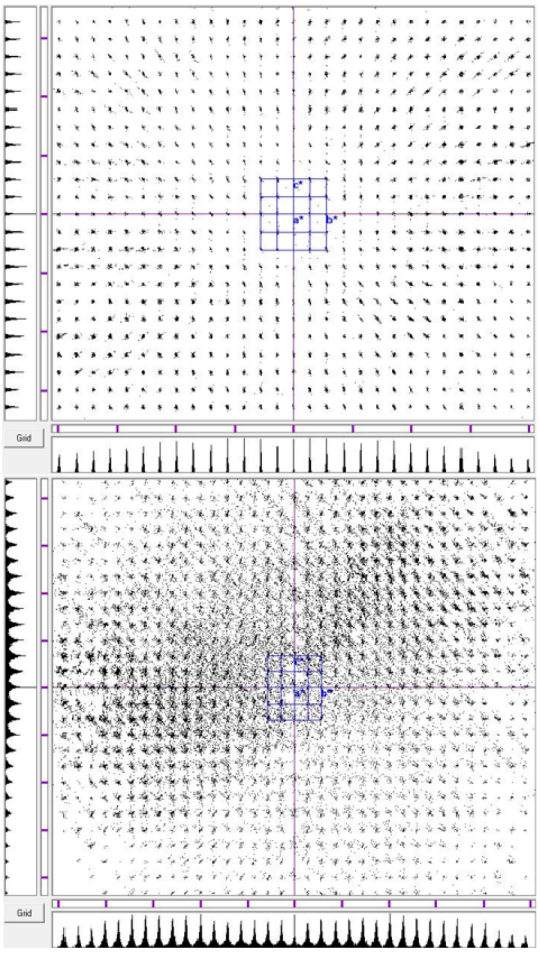

Figure 7. Reciprocal space plot along [100] for a crystal before (top) and after (bottom) storage in air for 3 d. Please note that each dot corresponds to one reflection with $I > 2\sigma(I)$. For reciprocal space plots in the other directions see Figures S13−S15.

DOI: 10.1021/acs.cgd.9b00727
Cryst. Growth Des. XXXX, XXX, XXX−XXX

This pattern is far from that of a single crystal, which would be expected in the case of a topotactic reaction, and therefore, we call this a pseudotopotactic reaction. Indexing of this pattern leads to a unit cell that is very similar to that obtained by XRPD, which indicates that compound **2** has formed (Table 1). The change in the unit cell volume is significantly larger than that obtained from the powder measurements, but it should be kept in mind that the XRPD measurements were performed at slightly elevated temperatures, where some thermal expansion already took place and that, in the geometry used for the synchrotron measurements, some deviations in the unit cell parameters can occur. However, it is obvious that correct integration of the intensities is difficult to achieve, and therefore, several different data sets were generated using different sizes of the integration box and different values for the mosaic spread, until the best reliability factors were obtained.

The structure cannot be refined using the atomic coordinates of **1** as starting model, but the structure could be easily solved in space group $P2_1/c$, and data refinement leads to a very similar structure model as that observed for **1**. The water content determined by single-crystal X-ray structure analysis is in good agreement with that determined by thermogravimetry. Surprisingly, the cyclam ligand, which is significantly disordered in **1**, is fully ordered in **2**. Moreover, not only some of the hydrate water molecules located between the layers are removed but also the two axial H_2O ligands of the $[Cu(cyclam)(H_2O)_2]^{2+}$ cations have been emitted, and the octahedral coordination is retained by bond formation between this Cu^{2+} cation and two terminal O atoms of two neighbored $\{[Cu(cyclam)]_2[HTiNb_9O_{28}]^{2-}\}$ anions, transforming the molecular structure into a one-dimensional network (Figure 8). The basicity of cluster O atoms is estimated from oxygen exchange rates accessible from ^{17}O NMR studies. Such studies were conducted on mono-, dititanoniobate, and decaniobate anions[54−56] demonstrating that terminal O atoms are the most basic ones. In agreement with this result the coordination of Cu^{2+} cations occurs to terminal O atoms of the cluster anion.

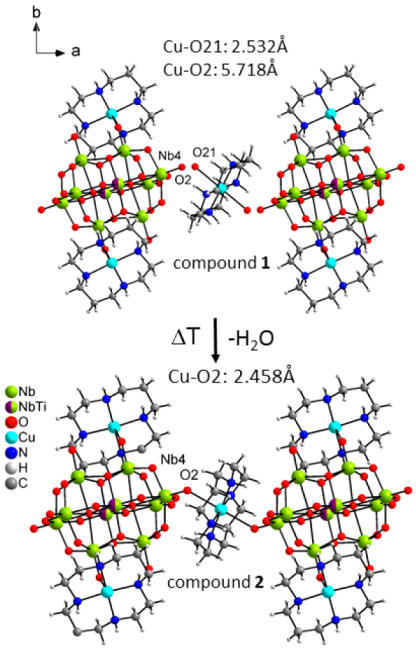

Figure 8. View of the structural changes during the transformation of **1** into **2**.

In **2** also a typical Jahn−Teller distortion is observed, but it is less pronounced than in compound **1**. The Cu−O bond length is reduced from 2.532 Å in **1** to 2.349(8) Å in **2**, indicating a much stronger interaction (Figure 8). Bond valence sum calculations revealed similar results as for **1** (Table S4), and the bond lengths and all geometrical parameters are also comparable to those obtained for **1** (Tables S5 and S6). It is noted that in **2** the distance between the Cu(II) cation and the terminal O atom that is involved in bond formation amounts to 2.349(8) Å, which rationalizes the enormous structural changes accompanied by the water removal (Figure 8). The dramatic decrease of the interlayer distance, the much stronger Cu−O interaction, and the ordering of the cyclam ligand strongly indicate that compound **2** is much more stable than compound **1**, and this might be the reason why no retransformation of **2** into **1** is observed if the sample is stored in a humid atmosphere. However, the structural reorganization generates chains with composition $\{[Cu(cyclam)]_3[HTiNb_9O_{28}]\}_n$, which are directed along [100] (Figure 9).

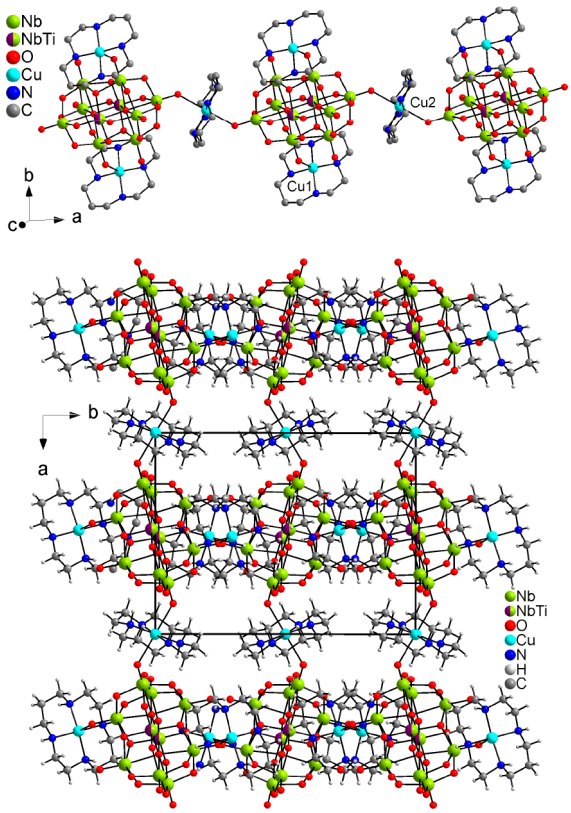

Figure 9. View of chains in **2** (top) and of the crystal structure of **2** along the crystallographic *c*-axis. H atoms as well as O atoms of H_2O molecules are omitted.

CONCLUSIONS

A new monotitano-nonaniobate compound (**1**) is reported consisting of $\{Cu(cyclam)]_2[HTiNb_9O_{28}]^{2-}\}$ anions that are arranged in layers, which are charge balanced by $[Cu(cyclam)(H_2O)_2]^{2+}$ cations that are located between the layers together with additional hydrate water molecules. The water can be removed, and this process occurs via a water-deficient phase as intermediate (**2**). XRPD investigations show a dramatic change

DOI: 10.1021/acs.cgd.9b00727
Cryst. Growth Des. XXXX, XXX, XXX−XXX

of the unit cell parameters indicating enormous structural changes, additionally indicating that predominantly the interlayer distance is shortened and that the anions within the layers rearrange and that therefore some structural relation should be present. Therefore, the water removal was investigated by single-crystal X-ray diffraction and, even if the diffraction pattern is far from that expected for a topotactic reaction, some order is present. A reasonable structure model was found for the intermediate phase, which especially shows that the coordinated water molecules of the isolated Cu^{2+} cation are replaced by terminal O atoms of the cluster, leading to the formation of chains and that the cyclam ligand that is disordered in **1** is fully ordered in **2**. Concerning the reaction mechanism occurring during the transformation of **2** into **1** in the presence of tiny amounts of water we cannot definitely exclude that crystals of **2** are partially dissolved and **1** recrystallizes from solution.

The present results suggest that new polyoxometalate compounds may be accessible by removal of solvent molecules that cannot be prepared applying other synthetic approaches. Moreover, we also presented a rare example that, even in those cases where, for example, XRPD indicates large structural changes, some structural relations and a smooth reaction pathway might be present, which in such a case should preferably be investigated by single-crystal X-ray diffraction.

■ ASSOCIATED CONTENT

Supporting Information

The Supporting Information is available free of charge on the ACS Publications website at DOI: 10.1021/acs.cgd.9b00727.

Tables with selected bond lengths and angles, results of BVS analyses, drawings of the structures, X-ray powder patterns, results of Pawley fits, TG, DTG, and DTA curves, and reciprocal space plots (PDF)

Accession Codes

CCDC 1919264−1919265 contain the supplementary crystallographic data for this paper. These data can be obtained free of charge via www.ccdc.cam.ac.uk/data_request/cif, or by emailing data_request@ccdc.cam.ac.uk, or by contacting The Cambridge Crystallographic Data Centre, 12 Union Road, Cambridge CB2 1EZ, UK; fax: +44 1223 336033.

■ AUTHOR INFORMATION

Corresponding Author

*E-mail: wbensch@ac.uni-kiel.de.

ORCID

Helge Reinsch: 0000-0001-5288-1135

Christian Näther: 0000-0001-8741-6508

Wolfgang Bensch: 0000-0002-3111-580X

Author Contributions

The manuscript was written through contributions of all authors. All authors have given approval to the final version of the manuscript.

Notes

The authors declare no competing financial interest.

■ ACKNOWLEDGMENTS

Financial support by the State of Schleswig-Holstein is gratefully acknowledged. Many thanks to DESY (Hamburg, Germany) for allocation of beamtime. Many thanks to Dr. Milan Köppen for providing the software to analyze the DESY data.

■ REFERENCES

(1) Frost, G. B.; Campbell, R. A. The Rate of Dehydration of Copper Sulphate Pentahydrate At Low Pressures of Water Vapor. *Can. J. Chem.* **1953**, *31*, 107−119.

(2) Garner, W. E.; Pike, H. V. Dehydration Nuclei on Crystals of Copper Sulphate Pentahydrate. *J. Chem. Soc.* **1937**, 1565−1568.

(3) Garner, W. E.; Tanner, M. G. X. -The dehydration of copper sulphate pentahydrate. *J. Chem. Soc.* **1930**, *0*, 47−57.

(4) Weiser, H. B.; Milligan, W. O.; Ekholm, W. C. The Mechanism of the Dehydration of Calcium Sulfate Hemihydrate. *J. Am. Chem. Soc.* **1936**, *58*, 1261−1265.

(5) Putnis, A.; Winkler, B.; Fernandez-Diaz, L. In situ IR spectroscopic and thermogravimetric study of the dehydration of gypsum. *Mineral. Mag.* **1990**, *54*, 123−128.

(6) Razouk, R. I.; Salem, A. S.; Mikhail, R. S. The Sorption of Water Vapor on Dehydrated Gypsum. *J. Phys. Chem.* **1960**, *64*, 1350−1355.

(7) Férey, G. A selective magnetic sponge. *Nat. Mater.* **2003**, *2*, 136−137.

(8) Nowicka, B.; Reczyński, M.; Rams, M.; Nitek, W.; Żukrowski, J.; Kapusta, C.; Sieklucka, B. Hydration-switchable charge transfer in the first bimetallic assembly based on the $[Ni(cyclam)]^{3+}$-magnetic CN-bridged chain $\{(H_3O)Ni^{III}(cyclam)Fe^{II}(CN)_6]\cdot 5H_2O\}_n$. *Chem. Commun.* **2015**, *51*, 11485−11488.

(9) Zhou, H.-C.; Long, J. R.; Yaghi, O. M. Introduction to metal-organic frameworks. *Chem. Rev.* **2012**, *112*, 673−674.

(10) Pinkowicz, D.; Podgajny, R.; Bałanda, M.; Makarewicz, M.; Gaweł, B.; Łasocha, W.; Sieklucka, B. Magnetic Spongelike Behavior of 3D Ferrimagnetic $\{Mn^{II}(imH)_2Nb^{IV}(CN)_8\}_n$ with T_c = 62 K. *Inorg. Chem.* **2008**, *47*, 9745−9747.

(11) Näther, C.; Greve, J.; Jeβ, I. New Coordination Polymer Changing Its Color upon Reversible Deintercalation and Reintercalation of Water. *Chem. Mater.* **2002**, *14*, 4536−4542.

(12) Schöllhorn, R.; Roer, W.; Wagner, K. Topotactic formation and exchange reactions of hydrated layered tin sulfides $A_x(H_2O)_ySnS_2$. *Monatsh. Chem.* **1979**, *110*, 1147−1152.

(13) Harvey, M. A.; Suarez, S.; Cukiernik, F. D.; Baggio, R. The topotactic dehydration of monoclinic $\{[Co(pht)(bpy)(H_2O)_2]\cdot 2H_2O\}_n$ into orthorhombic $[Co(pht)(bpy)(H_2O)_2]_n$ (pht is phthalate and bpy is 4,4′-bipyridine). *Acta Crystallogr., Sect. C: Struct. Chem.* **2014**, *70*, 978−982.

(14) Suckert, S.; Rams, M.; Rams, M. M.; Näther, C. Reversible and Topotactic Solvent Removal in a Magnetic $Ni(NCS)_2$ Coordination Polymer. *Inorg. Chem.* **2017**, *56*, 8007−8017.

(15) Englert, U.; Ganter, B.; Wagner, T.; et al. Reversible Topotactic Hydration and Dehydration of an Europium Complex. *Z. Anorg. Allg. Chem.* **1998**, *624*, 970−974.

(16) Long, D.-L.; Burkholder, E.; Cronin, L. Polyoxometalate clusters, nanostructures and materials: From self assembly to designer materials and devices. *Chem. Soc. Rev.* **2007**, *36*, 105−121.

(17) Long, D.-L.; Tsunashima, R.; Cronin, L. Polyoxometallate als Bausteine für funktionelle Nanosysteme. *Angew. Chem.* **2010**, *122*, 1780−1803.

(18) Nyman, M. Polyoxoniobate chemistry in the 21st century. *Dalton Trans.* **2011**, *40*, 8049−8058.

(19) Klemperer, W. G.; Marquart, T. A.; Yaghi, O. M. Neue Richtungen in der Polyvanadat-Chemie: Von Käfigen und Clustern zu Körben, Bändern, Schalen und Fässern. *Angew. Chem.* **1992**, *104*, 51−53; *Angew. Chem., Int. Ed. Engl.* **1992**, *31*, 49−51.

(20) Rhule, J. T.; Hill, C. L.; Judd, D. A.; Schinazi, R. F. Polyoxometalates in Medicine. *Chem. Rev.* **1998**, *98*, 327−357.

(21) Mizuno, N.; Misono, M. Heterogeneous Catalysis. *Chem. Rev.* **1998**, *98*, 199−218.

(22) Wutkowski, A.; Näther, C.; Kögerler, P.; Bensch, W. Antimonato polyoxovanadate based three-dimensional framework exhibiting ferromagnetic exchange interactions: Synthesis, structural characterization, and magnetic investigation of {[Fe-

DOI: 10.1021/acs.cgd.9b00727
Cryst. Growth Des. XXXX, XXX, XXX−XXX

$(C_6H_{14}N_2)_2]_3V_{15}Sb_6O_{42}(H_2O)\}\cdot 8H_2O$. *Inorg. Chem.* **2013**, *52*, 3280−3284.

(23) *Trends in Polyoxometalate Research;* Ruhlmann, L., Schaming, D., Eds.; Nova Science Publishers, Inc.: United States, 2015.

(24) Gumerova, N. I.; Rompel, A. Synthesis, structures and applications of electron-rich polyoxometalates. *Nat. Rev. Chem.* **2018**, *2*, 1−20.

(25) Wendt, M.; Warzok, U.; Näther, C.; van Leusen, J.; Kögerler, P.; Schalley, C. A.; Bensch, W. Catalysis of "outer-phase" oxygen atom exchange reactions by encapsulated "inner-phase" water in $\{V_{15}Sb_6\}$-type polyoxovanadates. *Chem. Sci.* **2016**, *7*, 2684−2694.

(26) Vilà-Nadal, L.; Cronin, L. Design and synthesis of polyoxometalate-framework materials from cluster precursors. *Nat. Rev. Mater.* **2017**, *2*, 1154.

(27) Mahnke, L. K.; Kondinski, A.; Warzok, U.; Näther, C.; van Leusen, J.; Schalley, C. A.; Monakhov, K. Y.; Kögerler, P.; Bensch, W. Configurational Isomerism in Polyoxovanadates. *Angew. Chem., Int. Ed.* **2018**, *57*, 2972−2975.

(28) Structure and Bonding in Molecular Vanadium Oxides: From Templates via Host-Guest Chemistry to Applications. In *Polyoxometalate-Based Assemblies and Functional Materials. Structure and Bonding;* Song, Y.-F., Ed.; Springer International Publishing Group, 2017.

(29) Monakhov, K. Y.; Bensch, W.; Koegerler, P. Semimetal-functionalised polyoxovanadates. *Chem. Soc. Rev.* **2015**, *44*, 8443−8483.

(30) Seliverstov, A.; Forster, J.; Heiland, M.; Unfried, J.; Streb, C. The anion-binding polyanion: A molecular cobalt vanadium oxide with anion-sensitive visual response. *Chem. Commun.* **2014**, *50*, 7840−7843.

(31) Nyman, M.; Bonhomme, F.; Alam, T. M.; Rodriguez, M. A.; Cherry, B. R.; Krumhansl, J. L.; Nenoff, T. M.; Sattler, A. M. A General Synthetic Procedure for Heteropolyniobates. *Science* **2002**, *297*, 996−998.

(32) Anderson, T. M.; Thoma, S. G.; Bonhomme, F.; Rodriguez, M. A.; Park, H.; Parise, J. B.; Alam, T. M.; Larentzos, J. P.; Nyman, M. Lithium Polyniobates. A Lindqvist-Supported Lithium-Water Adamantane Cluster and Conversion of Hexaniobate to a Discrete Keggin Complex. *Cryst. Growth Des.* **2007**, *7*, 719−723.

(33) Son, J.-H.; Ohlin, C. A.; Larson, E. C.; Yu, P.; Casey, W. H. Synthesis and Characterization of a Soluble Vanadium-Containing Keggin Polyoxoniobate by ESI-MS and ^{51}V NMR: $(TMA)_9[V_3Nb_{12}O_{42}] \cdot 18H_2O$. *Eur. J. Inorg. Chem.* **2013**, *2013*, 1748−1753.

(34) Alam, T. M.; Nyman, M.; Cherry, B. R.; Segall, J. M.; Lybarger, L. E. Multinuclear NMR Investigations of the Oxygen, Water, and Hydroxyl Environments in Sodium Hexaniobate. *J. Am. Chem. Soc.* **2004**, *126*, 5610−5620.

(35) Zhang, X.; Liu, S.-x.; Li, S.-j.; Gao, Y.-H.; Wang, X.-n.; Tang, Q.; Liu, Y.-w. Two Members of the $\{X_4Nb_{16}O_{56}\}$ Family (X = Ge, Si) Based on $[(GeOH)_2Ge_2Nb_{16}H_2O_{54}]^{12-}$ and $[K(GeOH)Ge_2Nb_{16}H_3O_{54}]^{10-}$. *Eur. J. Inorg. Chem.* **2013**, *2013*, 1706−1712.

(36) Huang, P.; Qin, C.; Wang, X.-L.; Sun, C.-Y.; Xing, Y.; Wang, H.-N.; Shao, K.-Z.; Su, Z.-M. A new organic-inorganic hybrid based on the crescent-shaped polyoxoanion $[H_6SiNb_{18}O_{54}]^{8-}$ and copper-organic cations. *Dalton Trans.* **2012**, *41*, 6075−6077.

(37) Son, J.-H.; Wang, J.; Osterloh, F. E.; Yu, P.; Casey, W. H. A tellurium-substituted Lindqvist-type polyoxoniobate showing high H_2 evolution catalyzed by tellurium nanowires via photodecomposition. *Chem. Commun.* **2014**, *50*, 836−838.

(38) Fullmer, L. B.; Mansergh, R. H.; Zakharov, L. N.; Keszler, D. A.; Nyman, M. Nb_2O_5 and Ta_2O_5 Thin Films from Polyoxometalate Precursors: A Single Proton Makes a Difference. *Cryst. Growth Des.* **2015**, *15*, 3885−3892.

(39) Jin, L.; Zhu, Z.-K.; Wu, Y.-L.; Qi, Y.-J.; Li, X.-X.; Zheng, S.-T. Record High-Nuclearity Polyoxoniobates: Discrete Nanoclusters $\{Nb_{114}\}$, $\{Nb_{81}\}$, and $\{Nb_{52}\}$, and Extended Frameworks Based on $\{Cu_3Nb_{78}\}$ and $\{Cu_4Nb_{78}\}$. *Angew. Chem., Int. Ed.* **2017**, *56*, 16288−16292.

(40) Shmakova, A. A.; Shiriyazdanov, R. R.; Karimova, A. R.; Kompankov, N. B.; Abramov, P. A.; Sokolov, M. N. Decay of Hexaniobate Complexes of Mn(IV) and Pt(IV) in Alkaline Solutions: Some New Hexaniobate Salts. *J. Cluster Sci.* **2018**, *29*, 1201−1207.

(41) Graeber, E. J.; Morosin, B. The Molecular Configuration of the Decaniobate Ion $(Nb_{10}O_{28}^{6-})$. *Acta Crystallogr., Sect. B: Struct. Crystallogr. Cryst. Chem.* **1977**, *33*, 2137−2143.

(42) Nyman, M.; Criscenti, L. J.; Bonhomme, F.; Rodriguez, M. A.; Cygan, R. T. Synthesis, structure, and molecular modeling of a titanoniobate isopolyanion. *J. Solid State Chem.* **2003**, *176*, 111−119.

(43) Dopta, J.; Krause, D.-C.; Näther, C.; Bensch, W. Controlling Fast Nucleation and Crystallization of Two New Polyoxoniobates. *Cryst. Growth Des.* **2018**, *18*, 4130−4139.

(44) Filowitz, M.; Ho, R. K. C.; Klemperer, W. G.; Shum, W. Oxygen-17 nuclear magnetic resonance spectroscopy of polyoxometalates. 1. Sensitivity and resolution. *Inorg. Chem.* **1979**, *18*, 93−103.

(45) Sheldrick, G. M. *SHELXS-97: Program for the Solution of Crystal Structures;* University of Goettingen: Goettingen, Germany, 1997.

(46) Sheldrick, G. M. *SHELXL-2014: Program for the Refinement of Crystal Structures;* University of Goettingen: Goettingen, Germany, 2014.

(47) Hammersley, A. P. *FIT2D: An Introduction and Overview*; ESRF97HA02T, 1997. Online at http://www.esrf.eu/computing/scientific/FIT2D/FIT2D_INTRO/fit2d.html

(48) Wu, H.-L.; Zhang, Z.-M.; Li, Y.-G.; Wang, X.-L.; Wang, E.-B. Recent progress in polyoxoniobates decorated and stabilized *via* transition metal cations or clusters. *CrystEngComm* **2015**, *17*, 6261−6268.

(49) Flynn, C. M.; Stucky, G. D. Sodium-6-Niobo-(ethylenediamine)cobaltate(III) and Its Chromate(III) Analog. *Inorg. Chem.* **1969**, *8*, 178−180.

(50) Carlson, G. A.; McReynolds, J. P.; Verhoek, F. H. Equilibrium Constants for the Formation of Ammine Complexes with Certain Metallic Ions. *J. Am. Chem. Soc.* **1945**, *67*, 1334−1339.

(51) Shen, L.; Li, C.-H.; Chi, Y.-N.; Hu, C.-W. $Zn(2,2'\text{-bipy})_2$/$Co(2,2'\text{-bipy})_2$ linked decaniobate $[Nb_{10}O_{28}]^{6-}$ clusters-zigzag neutral chains. *Inorg. Chem. Commun.* **2008**, *11*, 992−994.

(52) Niu, J.; Wang, G.; Zhao, J.; Sui, Y.; Ma, P.; Wang, J. Zero- or One-Dimensional Organic-Inorganic Hybrid Polyoxoniobates Constructed from Decaniobate Units and Transition-Metal Complexes. *Cryst. Growth Des.* **2011**, *11*, 1253−1261.

(53) Matsumoto, M.; Ozawa, Y.; Yagasaki, A. Reversible dimerization of decaniobate. *Polyhedron* **2010**, *29*, 2196−2201.

(54) Villa, E. M.; Ohlin, C. A.; Rustad, J. R.; Casey, W. H. Isotope-exchange dynamics in isostructural decametalates with profound differences in reactivity. *J. Am. Chem. Soc.* **2009**, *131*, 16488−16492.

(55) Villa, E. M.; Ohlin, C. A.; Balogh, E.; Anderson, T. M.; Nyman, M.; Casey, W. H. Reaction Dynamics of the Decaniobate Ion $[HxNb_{10}O_{28}]^{(6-x)-}$ in Water. *Angew. Chem.* **2008**, *120*, 4922−4924.

(56) Villa, E. M.; Ohlin, C. A.; Casey, W. H. Oxygen-isotope exchange rates for three isostructural polyoxometalate ions. *J. Am. Chem. Soc.* **2010**, *132*, 5264−5272.

DOI: 10.1021/acs.cgd.9b00727
Cryst. Growth Des. XXXX, XXX, XXX−XXX